Mean-field theory of a recurrent epidemiological model

Viktor Nagy
Department of Physics, Institute for Research in Electronics and Applied Physics, University of Maryland, College Park, Maryland 20742, USA
(Received 6 February 2009; published 9 June 2009)

Our purpose is to provide a mean-field theory for the discrete time-step susceptible-infected-recovered-susceptible (SIRS) model on uncorrelated networks with arbitrary degree distributions. The effect of network structure, time delays, and infection rate on the stability of oscillating and fixed point solutions is examined through analysis of discrete time mean-field equations. Consideration of two scenarios for disease contagion demonstrates that the manner in which contagion is transmitted from an infected individual to a contacted susceptible individual is of primary importance. In particular, the manner of contagion transmission determines how the degree distribution affects model behavior. We find excellent agreement between our theoretical results and numerical simulations on networks with large average connectivity.

DOI: 10.1103/PhysRevE.79.066105 PACS number(s): 89.75.Hc, 87.23.Ge, 05.70.Fh

I. INTRODUCTION

The effect of social connectivity structure on the behavior of infectious diseases [1] has been of great interest. An important goal of epidemiology is to reveal the connection between the network structure of social connections, the spreading rate of the disease, and the possibility of large epidemic outbreaks [2,3]. In particular, the degree distribution P_k, defined as the fraction of individuals having k connections to other individuals, is a key factor in determining the properties of epidemic spreading. A signature of epidemiological models is the presence of phase transitions, i.e., qualitative changes in behavior, as the degree distribution or spreading rate is changed [2,3]. For the intensively studied susceptible-infected-susceptible and susceptible-infected-recovered (SIR) epidemiological models, the phase transitions between prevalence and extinction of the disease can be analytically understood, for instance, by using methods of percolation theory [3]. Surprising consequences of these results are the lack of an epidemic threshold [4] and virtually instantaneous spread of the disease [5] for heavy tailed degree distributions.

The purpose of the present paper is to provide both analytical and numerical results on the discrete time-step susceptible-infected-recovered-susceptible (SIRS) network model [6]. In particular, our aim is to reveal the connection between model behavior and the underlying network structure. The SIRS model applies to diseases where individuals cannot obtain permanent resistance against the disease as a result of frequent mutations of the pathogen, e.g., influenza. The discrete time-step approach is justified because, on one hand, it is an approximation to the continuous time case, while on the other hand, our every day life has a certain periodicity, e.g., seasonal changes. For the discrete time-step SIRS model Kuperman and Abramson [6] illustrated the importance of network structure by implementing the model in the Watts-Strogatz framework [7]. It was found that for a regular network, (i.e., a topological ring, where each node has a fixed coordination number), the stationary state of the system is a stable fixed point. As network connections are rewired and random network structure is approached, the fixed point becomes unstable leading to the appearance of self-sustained oscillations. It was also conjectured that on uncorrelated networks the model leads to oscillatory behavior in most cases. In [8] the effect of community structure on the synchronization properties of the SIRS model was studied numerically. The presence of oscillatory states makes the SIRS model particularly interesting, as it provides an example of synchronization phenomena on networks. Qualitatively, similar phase transitions can be observed, for instance, in the well-known Kuramoto model [9].

To account for adaptive behavior in social interactions, recent work [10] proposed a model where the connection structure of the network and the disease itself evolve simultaneously in time. Using adaptive connection structure, susceptible individuals are able to avoid contact with infected ones by rewiring their network connections. Adaptive rewiring leads to regions of bistability, where either a prevalent, disease-free, or oscillatory phase can exist as illustrated for both SIR [10] and SIRS models [11].

In a previous theoretical work on the SIRS model, Girvan *et al.* [12] applied Cooke's discrete time-delay analysis [13] to model epidemics. Synchronization between coupled communities was examined in [14].

In the present paper, as an extension of previous numerical [6] and theoretical [12] works, we investigate the discrete time-step SIRS model on uncorrelated networks with arbitrary degree distributions and provide analytical and numerical results on the role of time delays, infection rate, and network structure. We intend to provide a better theoretical basis for the numerous simulation results [6,8]. It is demonstrated that the role of applied contagion scheme is of primary importance and that the model exhibits rich dynamical behavior, with oscillating solutions and fixed points. In particular, the contagion scheme determines the connection between network structure and model behavior. Moreover, while our theoretical results apply for an annealed case, assuming a well mixed population, we find good agreement with the numerical simulations for a fixed network structure, provided the average connectivity of the network is sufficiently large.

The outline of the paper is the following. In Sec. II, we provide a framework for the following theoretical discussion.

In Secs. III and IV, we examine the analytical properties of the two most commonly used contagion schemes. In Sec. V, we compare the obtained results with numerical simulations of the model on a network with fixed connection structure. Finally, in Sec. V we summarize our results and give conclusions.

II. FRAMEWORK

We study a model of infectious disease that has three stages: susceptible S, infected I, and recovered R [6]. Each individual of the population is represented by a node of the network categorized into one of these three stages. Interactions between elements of the population are described by the network connections, and infection can proceed through them. Each element i in the network is characterized by a discrete time counter $\tau_i=0,1,\ldots,\tau_I+\tau_R$, describing the phase of the disease. Movement between the classes is governed by the following rules. A susceptible (S) element i, whose time counter is by definition $\tau_i=0$, can become infected if connected to an infected (I) individual. Once infected, the node deterministically goes through a cycle that lasts $\tau_I+\tau_R$ time steps. In the first τ_I time steps i is infected and can transmit the disease to its susceptible neighbors. In the following τ_R time steps, infected individuals pass to the recovered state (R) where individuals are not contagious and are also immune to the disease. The cycle is finally completed when individuals return to the susceptible state and their time counter is set to zero.

Our next step is to specify how infection spreads from an infected to a susceptible individual along network connections. In the present paper we consider two scenarios for disease contagion. The motivation behind this is that the given framework can be applied to a variety of situations, e.g., epidemic dynamics in the human population or computer virus spreading on networks. It is a realistic assumption that local interaction structure in these cases can be quite different. It is essential to understand both the common features and differences arising from implementing different spreading schemes.

For definition of contagion schemes [6], we consider a susceptible node with connectivity k and k_{inf} infected neighbors. Furthermore, we assume that infection probability can be characterized by a positive spreading rate $0<\mu\leq 1$. In the first scenario, which is referred to as linear, the probability that the susceptible node becomes infected in a single time step is $\mu k_{inf}/k$. Specifically, a node becomes infected with probability μ if all of its neighbors are infected. (Previous work [6] for this scheme does not involve the parameter μ, which is equivalent to taking $\mu=1$.) In the second scenario, referred to nonlinear, we assume that each infected node spreads the disease to its susceptible neighbors with probability μ. Thus, the probability of infection of the susceptible node by its infected neighbors at a given time step is $1-(1-\mu)^{k_{inf}}$. We note that the linear contagion scheme is best understood as an approximation to the nonlinear scenario $1-(1-\mu/k)^{k_{inf}}$ for small μ/k.

The time dependence of network structure is a crucial problem that needs to be addressed. Within the framework of uncorrelated networks, we can visualize two fundamentally different approaches. One possibility is when the network connections are fixed in time. This situation is relevant when the time scale of disease spreading is much faster than the time scale that characterizes the creation and destruction of new network connections. This situation, for instance, can describe the spread of computer viruses on the internet. Another option is to consider annealed connection structure, i.e., the network connections are randomly rewired in every time step, while keeping the coordination number of each node constant. This assumption is justified if the social interaction structure of the population is dominated by random encounters. In reality, every person has a number of fixed connections, e.g., family members and colleagues, but also interacts randomly with the rest of the population, e.g., while using public transportation. Connectivity of an individual characterizes both fixed connections and random interactions, where in the annealed approach the latter is assumed to be more significant.

In the following theoretical discussion we use annealed approach, assuming that random encounters dominate. While the annealed network structure is meaningful in itself, it also provides a mean-field approximation to the fixed case. In Sec V. we will show that the differences arising from these two approaches disappear, provided that the average connectivity of the network is larger than a threshold.

Every uncorrelated network can be fully characterized by its degree distribution P_k, where P_k is the fraction of nodes with connectivity k. The state of the system is updated in discrete time steps. In each time step a fraction of susceptible individuals can become infected. The fraction of nodes that have connectivity k and become infected at time step t is denoted $i_k(t)$. As each infected individual spends exactly τ_I time steps in the infected state and τ_R time steps in the recovered state, the fractions of infected, recovered, and susceptible nodes with connectivity k, denoted I_k, R_k, and S_k, respectively, equal to

$$I_k(t)=\sum_{t'=0}^{\tau_I-1} i_k(t-t'), \tag{1}$$

$$R_k(t)=\sum_{t'=\tau_I}^{\tau_I+\tau_R-1} i_k(t-t'), \tag{2}$$

$$S_k(t)=P_k-I_k-R_k=P_k-\sum_{t'=0}^{\tau_I+\tau_R-1} i_k(t-t'). \tag{3}$$

By definition of uncorrelated networks, when we follow a randomly chosen edge to one of its end points, the probability that we get to node with connectivity k is simply $kP_k/\langle k\rangle$, independent of the node the edge started from. Here we used the notation $\langle k\rangle=\Sigma_h hP_h$. This is an expression of the fact that high-degree vertices have more edges attached to them than low-degree ones. In annealed networks, infected nodes also form an uncorrelated network, which implies that if one follows a randomly chosen edge to one of its end points, then the probability that the chosen edge goes to an infected node

with connectivity k is $kI_k(t)/\langle k\rangle$. For convenience, we introduce the following notations:

$$\langle k\rangle_i(t) = \sum_k k i_k(t), \tag{4}$$

$$\langle k\rangle_I(t) = \sum_k k I_k(t) = \sum_{t'=0}^{\tau_I - 1} \langle k\rangle_i(t-t'). \tag{5}$$

Thus, $\langle k\rangle_i(t)$ is the average degree of nodes that first become infected at time t and $\langle k\rangle_I(t)$ is the average degree of the population of all nodes in the infected state at time t. Obviously we have $\langle k\rangle_i(t) \leq \langle k\rangle_I(t)$ and $\langle k\rangle_I(t) \leq \langle k\rangle$. The probability that a given end point of a random edge is connected to an infected neighbor,

$$q(t) = \sum_k k I_k(t)/\langle k\rangle = \langle k\rangle_I(t)/\langle k\rangle. \tag{6}$$

The probability that a node with connectivity k has exactly x infected neighbors is given by the binomial distribution,

$$b(k,x) = \binom{k}{x} q(t)^x [1-q(t)]^{k-x}. \tag{7}$$

If a susceptible node has exactly x infected neighbors, then the probability of infection is by definition $\mu x/k$ in the linear and $1-(1-\mu)^x$ in the nonlinear case. Taking the expectation value of $\mu x/k$ with respect to the above defined binomial distribution yields the result that a susceptible node with connectivity k is infected with probability $\mu q(t)$ in one time step. (That is, the probability that a susceptible node with x infected neighbors is not infected is $1-\mu x/k$, and the probability that the node has exactly x infected neighbors is given by the binomial distribution $b(k,x)$ [Eq. (7)]. Thus, the probability that infection occurs is $\mu q(t) = 1 - \Sigma_x b(k,x)(1-\mu x/k)$.) For the nonlinear contagion scheme this probability is $1-[1-\mu q(t)]^k$. We can now formulate our discrete time dynamical equations. The fraction of nodes infected at time step $t+1$ equals the fraction of susceptible nodes multiplied by the probability of infection,

$$i_k(t+1) = \mu \frac{\langle k\rangle_I(t)}{\langle k\rangle} S_k(t), \tag{8}$$

for the linear contagion scheme and

$$i_k(t+1) = \left[1 - \left(1 - \mu \frac{\langle k\rangle_I(t)}{\langle k\rangle}\right)^k\right] S_k(t), \tag{9}$$

for the nonlinear contagion scheme, where $\langle k\rangle_I(t)$ and $S_k(t)$ are given by Eqs. (3) and (5). Equations (8) and (9) define discrete dynamical systems for the variables $i_k(t)$. It is worth noting that if only one connectivity is present in the degree distribution, i.e., $P[k] = \delta_{k,k_0}$ for some k_0, and we choose $\tau_I = 1, \tau_R = 0$, then Eq. (8) simplifies to the logistic map. Equations (8) and (9), similarly to the logistic map, show chaotic behavior in certain parameter regions, period doubling, etc. Here, however, we restrict our attention to study the transition from fixed points to solutions with explicit time dependence.

In the present paper, our main interest is to understand the interplay between network structure and the statistically steady state of the disease. From this perspective, we distinguish three qualitatively different long time scenarios: (i) the disease can die out, resulting in every node becoming susceptible; (ii) the disease can become prevalent resulting in the average number of infected individuals becoming constant in time; or (iii) the disease can become prevalent with sustained oscillations. The first two scenarios correspond to fixed points of the maps [Eqs. (8) and (9)], trivial $i_k(t) = 0$ and nontrivial $i_k(t) > 0$, respectively, while oscillating solutions are characterized by the instability of both fixed points. We note that oscillating solutions of Eqs. (8) and (9) are rarely periodic and what we can observe, in general, is quasiperiodic behavior.

In Secs. III and IV, we examine the existence and the linear stability of solutions for both contagion schemes. The boundary that encompasses the stability regions of the two fixed points will be a curve where the system undergoes a Neimark bifurcation.

III. LINEAR CONTAGION SCHEME

A. Fixed points

Our purpose is to understand how the degree distribution (P_k), time delays (τ_I, τ_R), and infection probability μ affect the stability of prevalent, extinct, and oscillating solutions of discrete dynamical system (8). The first step in the following analysis is to determine the fixed points corresponding to map (8). Insertion of Eqs. (1) and (3) into Eq. (8) yields

$$i_k(t+1) = \mu \frac{\sum_{t'=0}^{\tau_I - 1} \langle k\rangle_i(t-t')}{\langle k\rangle} \left(P_k - \sum_{t'=0}^{\tau_I+\tau_R-1} i_k(t-t')\right), \tag{10}$$

where $\langle k\rangle_i(t) = \Sigma_h h i_h(t)$. Fixed points of the system, denoted i_k^*, are time independent and fulfill the equation

$$i_k^* = \frac{\mu \tau_I \langle k\rangle_i^*}{\langle k\rangle} [P_k - (\tau_R + \tau_I) i_k^*]. \tag{11}$$

The trivial solution $i_k^* = 0$ always exits and is the only solution if the infection rate μ equals zero. We have the self-consistency relation

$$\langle k\rangle_i^* = \sum_k k i_k^* = \frac{\mu \tau_I \langle k\rangle \langle k\rangle_i^*}{\langle k\rangle + \mu(\tau_I + \tau_R)\tau_I \langle k\rangle_i^*}, \tag{12}$$

which for $\langle k\rangle_i^* \neq 0$ can be solved explicitly to yield

$$\langle k\rangle_i^* = \frac{\langle k\rangle}{\tau_I + \tau_R}\left(1 - \frac{1}{\mu \tau_I}\right), \tag{13}$$

$$i_k^* = \frac{P_k}{\tau_I + \tau_R}\left(1 - \frac{1}{\mu \tau_I}\right). \tag{14}$$

According to Eqs. (13) and (14) the distribution of infected nodes is proportional to P_k. I_k and S_k are related to i_k^* via the

relationships $I_k=\tau_I i_k^*$ and $R_k=\tau_I i_k^*$. Furthermore, because both i_k^* and $\langle k\rangle_i^*$ are necessarily positive quantities, for $0\leq\mu\leq 1/\tau_I$, only the trivial ($i_*^k=0$) solution exists. The critical infection probability, denoted μ_0, marks the epidemic threshold of the disease, and it is independent of network parameters

$$\mu_0 = 1/\tau_I. \tag{15}$$

Since for $\mu>\mu_0$ both solutions exist and could be stable simultaneously, stability analysis is required to determine the system's behavior. Linear stability of the fixed points can be obtained by adding a small perturbation, $i_k(t)=i_k^*+\delta i_k(t)$, and neglecting terms beyond linear order,

$$\delta i_k(t+1) = \mu\frac{P_k-(\tau_I+\tau_R)i_k^*}{\langle k\rangle}\sum_{t'=0}^{\tau_I-1}\delta\langle k\rangle_i(t-t') - \frac{\mu\tau_I\langle k\rangle_i^*}{\langle k\rangle}\sum_{t'=0}^{\tau_I+\tau_R-1}\delta i_k(t-t'). \tag{16}$$

Due to the presence of the terms $\delta\langle k\rangle_i(t-t')$, Eq. (16) is not independent. The analysis, however, can be considerably simplified if we multiply both sides by k and sum over k,

$$\delta\langle k\rangle_i(t+1) = \mu\frac{\langle k\rangle-(\tau_I+\tau_R)\langle k\rangle_i^*}{\langle k\rangle}\sum_{t'=0}^{\tau_I-1}\delta\langle k\rangle_i(t-t') - \frac{\mu\tau_I\langle k\rangle_i^*}{\langle k\rangle}\sum_{t'=0}^{\tau_I+\tau_R-1}\delta\langle k\rangle_i(t-t'). \tag{17}$$

With the notation

$$a = \mu-\mu(\tau_I+\tau_R)\langle k\rangle_i^*/\langle k\rangle, \tag{18}$$

$$b = -\mu\tau_I\langle k\rangle_i^*/\langle k\rangle, \tag{19}$$

and $x_t=\delta\langle k\rangle_i(t)$ we can rewrite Eq. (17),

$$x_{t+1} = a\sum_{t'=0}^{\tau_I-1}x_{t-t'} + b\sum_{t'=0}^{\tau_I+\tau_R-1}x_{t-t'}, \tag{20}$$

where $a=\mu$ and $b=0$ for the trivial and $a=1/\tau_I$ and $b=-(\mu\tau_I-1)/(\tau_I+\tau_R)$ for the nontrivial solutions given by Eqs. (13) and (14). Surprisingly, both a and b are independent of P_k. As a result, stability of the fixed points is determined only by the time delays τ_I, τ_R and μ. Hence, for linear contagion the underlying network structure is unimportant, in contrast with the nonlinear scheme, where the role of degree distribution is essential, as we will see in Sec V.

B. Shur stability

Equation (20) defines a linear $\tau_I+\tau_R$-dimensional discrete time dynamical system. We devote some time to examine its stability properties for arbitrary a and b because the general results obtained will be used in the rest of the paper. In order to determine the a, b pairs, where linear system (20) is stable, we look for eigensolutions of Eq. (17), in the form $x_t=x_0\lambda^t$ for complex λ, leading to the algebraic equation

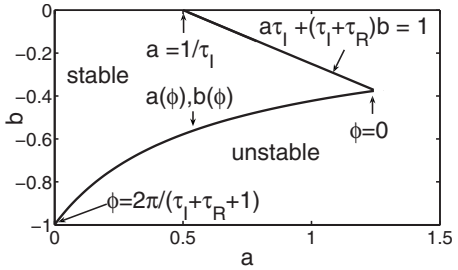

FIG. 1. Stability regions for Eq. (21) for $\tau_I=2$ and $\tau_R=2$. The straight line starting from point $(a,b)=(1/\tau_I,0)$ corresponds to the equation $a\tau_I+b(\tau_I+\tau_R)=1$, while the curve is given by Eqs. (22) and (23).

$$\lambda = a\sum_{r=0}^{\tau_I-1}\lambda^{-r} + b\sum_{r=0}^{\tau_I+\tau_R-1}\lambda^{-r}. \tag{21}$$

Dynamical system (20) is stable if all roots of polynomial (21) have absolute value smaller than one. Since $a\geq 0$ and $b\leq 0$, we can restrict our attention to the lower right quarter of the (a,b) plane. Possible boundaries between stability and instability can be determined by looking for solutions of Eq. (21) on the complex unit circle $\lambda=e^{i\phi}$. If $\phi=0$, we obtain $1=\tau_I a+(\tau_I+\tau_R)b$. If, however, $\phi\neq 0$, we can sum the trigonometric series in Eq. (21) to obtain

$$a(\phi) = \frac{\sin[(\tau_I+\tau_R+1)\phi/2]\sin(\phi/2)}{\sin(\tau_I\phi/2)\sin(\tau_R\phi/2)}, \tag{22}$$

$$b(\phi) = -\frac{\sin[(\tau_I+1)\phi/2]\sin(\phi/2)}{\sin[(\tau_I+\tau_R)\phi/2]\sin(\tau_R\phi/2)}. \tag{23}$$

Equations (22) and (23) for $0\leq\phi\leq 2\pi$ represent a discontinuous curve that divides the (a,b) plane into stable and unstable regions. At this point, however, we do no know which of these regions correspond to stable (a,b) pairs. An analytical solution to this problem can be worked out using Shur's theorem as given in Appendix, Sec. I. Also see [15]. Here, we omit this part and determine the nature of the relevant regions numerically. Stability regions of Eq. (20) in the lower right quarter plane are shown in Fig. 1. The curves encompassing the region of stability can be easily identified. The line corresponds to $1=\tau_I a+(\tau_I+\tau_R)b$, while the curve starting at the point $(a,b)=(0,-1)$ is given by $\phi\rightarrow[a(\phi),b(\phi)]$, as defined in Eqs. (22) and (23). The parametric curve intersects the $1=\tau_I a+(\tau_I+\tau_R)b$ line at $\phi=0$ and the $a=0$ axis at $\phi=2\pi/(\tau_I+\tau_R+1)$.

C. Phase diagram

As the line $a\tau_I+b(\tau_I+\tau_R)=1$ intersects the $b=0$ axis at $a=1/\tau_I$, the stability criterion for the trivial solution ($a=\mu, b=0$) is $a=\mu<1/\tau_I=\mu_0$, i.e., the trivial fixed point is unstable whenever the nonzero solution exists. A remarkable feature of this critical point is that it is determined exclusively by τ_I. For nontrivial solutions (13) and (14), on the other hand, we have $a=1/\tau_I$, $b=-(\mu\tau_I-1)/(\tau_I+\tau_R)$, which defines a vertical line starting at $a=1/\tau_I$ as shown in Fig. 2.

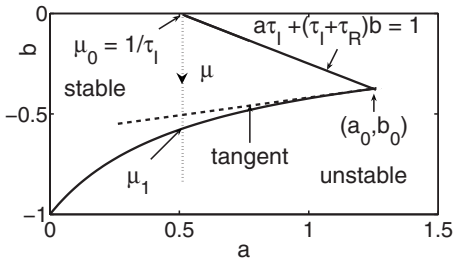

FIG. 2. Approximation of the border of stability region with a tangent starting at point (a_0,b_0) for $\tau_I=2$ and $\tau_R=2$.

The critical value of μ where this line intersects the unstable region, denoted μ_1, marks the Neimark-bifurcation point where oscillating solutions emerge. If $\mu_1>1$ for fixed τ_I and τ_R, then oscillations do not occur. We can obtain a simple approximation for μ_1 by taking the tangent of the parametric curve at $\phi=0$, point (a_0,b_0) as shown in Fig. 2, and calculating μ where this tangent intersects the line given by $a=1/\tau_I$ and $b=-(\mu\tau_I-1)/(\tau_I+\tau_R)$. A simple calculation yields

$$\frac{\mu_1-\mu_0}{\mu_0} \approx \frac{2(\tau_I+1)}{\tau_R+1} \quad \text{for } \tau_R > \tau_I \text{ and } \mu_0 = \frac{1}{\tau_I}. \tag{24}$$

Details of the derivation are discussed in Appendix, Sec. II. We note that the accuracy of Eq. (24) improves with increasing τ_R and it provides an excellent approximate value for μ_1. A simple consequence of Eq. (24) is that μ_1 converges to $\mu_0=1/\tau_I$ as $\tau_R\to\infty$, and for large τ_R the region where prevalence exists without oscillations disappears.

We summarize our results in Fig. 3 for $\tau_I=4$. Regions corresponding to prevalence, extinction, and oscillatory solutions are shown as functions of μ and τ_R. The solid line separating the oscillatory and prevalent regions represents the full numerical solution of Eq. (17), while the dashed curve represents approximation (24). We find excellent quantitative agreement. The infection rate μ_1 asymptotically approaches $\mu_0=1/\tau_I$. Moreover, if $\tau_I=2$, then for $\tau_R\leq 4$ we do not have an oscillatory phase for any $\mu\leq 1$. In general, for a given τ_I we need a minimum number of time steps spent in the recovered phase to observe oscillations, in good agreement with Eq. (24).

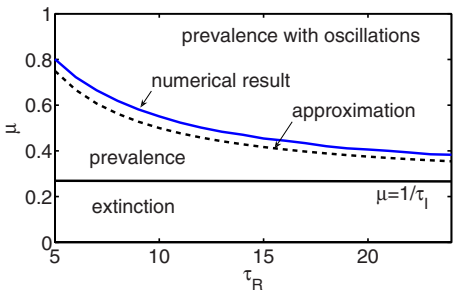

FIG. 3. (Color online) Phase portrait of Eq. (10) with $\tau_I=4$. The solid curve separating oscillatory and prevalent solutions is obtained from full numerical solution of Eq. (10), while the dotted curve is given by Eq. (24).

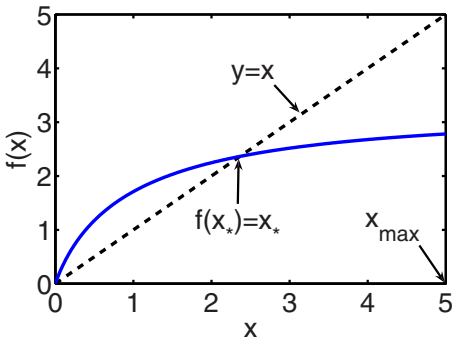

FIG. 4. (Color online) Solution of the fixed point problem $x=f(x)$, where $f(x)$ is given by Eq. (26).

IV. NONLINEAR SCHEME

We have seen in Sec. III C that emergence of prevalent and oscillatory solutions for linear contagion was independent of the degree distribution. Introduction of nonlinearity, however, leads to explicit dependence on the network structure. In this section, we first explore the properties of the nontrivial fixed points, and we then turn to presentation of the analytical characterization of the oscillatory phase.

A. Fixed points

The discrete time dynamical system in this case is given by Eq. (9). Its fixed points, denoted i_k^*, must satisfy

$$i_k^* = P_k \frac{1-\left(1-\tau_I\mu\dfrac{\langle k\rangle_i^*}{\langle k\rangle}\right)^k}{1+(\tau_I+\tau_R)-(\tau_I+\tau_R)\left(1-\tau_I\mu\dfrac{\langle k\rangle_i^*}{\langle k\rangle}\right)^k}. \tag{25}$$

Equation (25) provides solutions in terms of the parameter $\langle k\rangle_i^*$. With the introduction of $f(x)$,

$$f(x) = \sum_h \frac{hP_h\left[1-\left(1-\tau_I\mu\dfrac{x}{\langle k\rangle}\right)^h\right]}{1+(\tau_I+\tau_R)-(\tau_I+\tau_R)\left(1-\tau_I\mu\dfrac{x}{\langle k\rangle}\right)^h}, \tag{26}$$

the self-consistency requirement, $\Sigma_h hi_k^*=\langle k\rangle_i^*$, is equivalent to the fixed point problem $f(x_*)=x_*$, where $x_*=\langle k\rangle_i^*$ as shown in Fig. 4. $f(0)=0$ is always satisfied, and, for $x_{\max}\equiv\langle k\rangle/\mu\tau_I$, we have the inequality

$$f(x_{\max}) = \frac{\langle k\rangle}{\tau_I+\tau_R+1} < x_{\max}. \tag{27}$$

Furthermore, because $f(x)$ is concave ($f''<0$), $f(x)$ intersects the x line at a point $x>0$ if and only if $f'(0)>1$, yielding the existence condition $f'(0)=\mu\tau_I\langle k^2\rangle/\langle k\rangle\geq 1$. As a result, for a given degree distribution we obtain the epidemic threshold,

$$\mu_0 = \frac{\langle k\rangle}{\tau_I\langle k^2\rangle}. \tag{28}$$

Equation (28) agrees with the result obtained for the SIR model [4] if we choose specifically $\tau_I=1$. An important con-

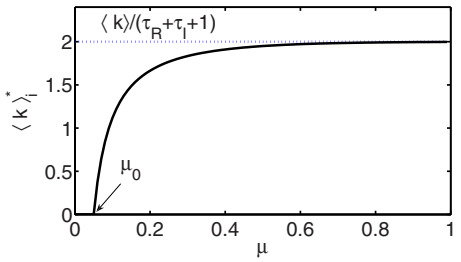

FIG. 5. (Color online) Stability regions for the nonlinear scheme as a function of τ_R and infection probability μ for $\tau_I=2$. Results for the full numerical simulation (solid curve) are compared to the approximation corresponding to Eq. (41) (dashed curve) for the degree distribution $P_k=\delta_{k,10}$.

sequence of Eq. (28) is that for divergent $\langle k^2\rangle$ we get $\mu_0=0$, e.g., for a power-law degree distribution $P_k\sim k^{-\gamma}$, with exponent $\gamma<3$, any nonzero infection probability leads to an epidemic outbreak, provided that the network has infinitely many nodes.

Since the nonzero fixed point $f(x_*)=x_*$ is attractive $[f'(x_*)<1]$, successive application of the map for any $x_0\neq 0$ converges to the solution $x_*=\lim_{n\to\infty} f^n(x_0)$. It is easy to see that $\langle k\rangle_i^*$ is an increasing function of μ (its derivative is given explicitly in Appendix, Sec. II.) and, under conditions discussed below, it asymptotically approaches $\langle k\rangle_i^{\max}=\langle k\rangle/(\tau_R+\tau_I+1)$, as shown in Fig. 5. Indeed, this asymptotic behavior is valid if $|x-f(x)|_{\mu=1}\ll 1$ at $x=\langle k\rangle/(\tau_R+\tau_I+1)$. Using the explicit form of $f(x)$ this condition is satisfied if $\Sigma_h hP_h[\tau_R/(\tau_R+\tau_I)]^h\ll\langle k\rangle$.

Motivated by the results of linear case (13), we approximate $\langle k\rangle_i^*$ with $\langle k\rangle_i^*\simeq a+b/\mu$, which, considering the asymptotic behavior of $\langle k\rangle_i^*$ and the condition $\langle k\rangle_i^*|_{\mu=\mu_0}=0$, yields

$$\langle k\rangle_i^* \simeq \frac{\langle k\rangle}{\tau_I+\tau_R+1}\left(1-\frac{\mu_0}{\mu}\right)\frac{1}{1-\mu_0} \quad \text{for} \quad \mu\geq\mu_0. \tag{29}$$

We will not provide rigorous proof of Eq. (29) but note that it agrees with the exact solution within 5% provided $\Sigma_h hP_h[\tau_R/(\tau_R+\tau_I)]^h\ll\langle k\rangle$. Accordingly, the fraction of infected individuals can be approximated by

$$I^* \simeq \frac{\tau_I}{\tau_I+\tau_R+1}\left(1-\frac{\mu_0}{\mu}\right)\frac{1}{1-\mu_0} \quad \text{for} \quad \mu\geq\mu_0. \tag{30}$$

We will compare Eq. (30) with experimental results in Sec. V.

B. Stability

After obtaining existence condition for the time-independent solutions of the discrete time dynamical equations we now turn to examine their stability. Adding a small perturbation to i_k^*, i.e., $i_k(t)=i_k^*+\delta i_k(t)$, and neglecting terms beyond linear order yields

$$\delta i_k(t+1)=\left(\sum_{t'=0}^{\tau_I-1}\delta\langle k\rangle_i(t-t')\right)a_k-b_k\sum_{t'=0}^{\tau_I+\tau_R-1}\delta i_k(t-t'), \tag{31}$$

where

$$a_k=\frac{k\mu}{\langle k\rangle}[P_k-(\tau_I+\tau_R)i_k^*]\left(1-\tau_I\mu\frac{\langle k\rangle_i^*}{\langle k\rangle}\right)^{k-1}, \tag{32}$$

$$b_k=1-\left(1-\tau_I\mu\frac{\langle k\rangle_i^*}{\langle k\rangle}\right)^k. \tag{33}$$

An important difference between Eqs. (31) and (17) is that b_k's depend explicitly on the coordination number k, and, unless $P_k=\delta_{k,k_0}$ for some k_0, we cannot handle the problem analytically in its full generality. Nevertheless, the trivial case ($\langle k\rangle_i^*=0$) can be solved exactly. If $\langle k\rangle_i^*=0$, then Eq. (31) yields

$$\delta i_k(t+1)=\left(\sum_{t'=0}^{\tau_I-1}\delta\langle k\rangle_i(t-t')\right)\frac{k\mu}{\langle k\rangle}P_k. \tag{34}$$

Multiplying both sides by k and summing, we obtain

$$\delta\langle k\rangle_i(t+1)=\left(\sum_{t'=0}^{\tau_I-1}\delta\langle k\rangle_i(t-t')\right)\frac{\langle k^2\rangle\mu}{\langle k\rangle}, \tag{35}$$

which is Eq. (20) with $b=0$ and $a=\mu\langle k^2\rangle/\langle k\rangle$. As discussed in Sec. III A, the condition for stability in this case is $a=\mu\langle k^2\rangle/\langle k\rangle<1/\tau_I$ or equivalently $\mu<\mu_0$. Therefore, the trivial fixed point is unstable whenever the nonzero solution exists. If $\delta i_k(t)\neq 0$, then we look for eigensolutions of Eq. (31) in the form $\delta i_k(t)=r_k\lambda^t$. Substitution of $\delta i_k(t)=r_k\lambda^t$ into Eq. (31) yields

$$r_k=\frac{a_k\sum_h hr_h}{\lambda+b_k\sum_{t'=0}^{\tau_I-1}\lambda^{-t'}}\sum_{t'=0}^{\tau_I+\tau_R-1}\lambda^{-t'}. \tag{36}$$

Multiplying both sides of Eq. (36) with k and summing lead to the self-consistency relation,

$$1=\sum_h\frac{ha_h}{\lambda+b_h\sum_{t'=0}^{\tau_I+\tau_R-1}\lambda^{-t'}}\sum_{t'=0}^{\tau_I-1}\lambda^{-t'}. \tag{37}$$

In particular, the system is stable if all λ solutions of Eq. (37) lie inside the complex unit cycle. Since $b_k=0$ at $\mu=\mu_0$ for all k, we can obtain a perturbative solution of Eq. (37) for $\mu-\mu_0\ll 1$, $b_k\ll 1$ as follows. For $b_k=0$ we obtain the zeroth-order expression,

$$\frac{\lambda}{\sum_h h a_h} = \sum_{t'=0}^{\tau_I - 1} \lambda^{-t'}. \tag{38}$$

If $b_k \approx 0$, we take the first-order approximation of the quotient in Eq. (37), i.e., $1/(1+b_h \sum_{t'=0}^{\tau_I+\tau_R-1} \lambda^{-t'-1}) \simeq 1 - b_h \sum_{t'=0}^{\tau_I+\tau_R-1} \lambda^{-t'-1}$, to obtain

$$\lambda = \sum_h h a_h \sum_{t'=0}^{\tau_I - 1} \lambda^{-t'} - \sum_h h a_h b_h \sum_{t'=0}^{\tau_I+\tau_R-1} \lambda^{-t'} \sum_{t'=0}^{\tau_I - 1} \lambda^{-t'-1}. \tag{39}$$

Finally, we replace the sum $\Sigma_{t'=0}^{\tau_I-1} \lambda^{-t'-1}$ in the second (perturbative) term with Eq. (38),

$$\lambda = \sum_h h a_h \sum_{t'=0}^{\tau_I - 1} \lambda^{-t'} - \frac{\sum_h h a_h b_h}{\sum_h h a_h} \sum_{t'=0}^{\tau_I+\tau_R-1} \lambda^{-t'}. \tag{40}$$

Note that Eq. (40) is exact if $P_k = \delta_{k,k_0}$ for some k_0. Introducing the notation $a = \Sigma_h h a_h$ and $b = \Sigma_h h a_h b_h / \Sigma_h h a_h$, polynomial (40) corresponds exactly to Eq. (21), and therefore the results obtained for its stability in Sec. III can be applied. Since for $\mu - \mu_0 \ll 1$ we have $b_k \sim k(\mu - \mu_0)$, we can expect Eq. (40) to be a good approximation if the network has few highly connected nodes. We also find that the accuracy of Eq. (40) improves with increasing τ_R. We have $a = 1/\tau_I$ and $b = 0$ at $\mu = \mu_0$, independent of the degree distribution, and the curve $\mu \to [a(\mu), b(\mu)]$ intersects the $b=0$ axis with a tangent $db/da = 2\tau_I$ (see Appendix, Sec. II). The infection probability where the curve $\mu \to [a(\mu), b(\mu)]$ enters the instability region of Eq. (40) is the Neimark-bifurcation point μ_1. For $\mu - \mu_0 \ll 1$, we can substitute a and b with their first-order Taylor expansion (given in Appendix, Sec. II) and follow the same argument that leads to Eq. (24) (i.e., approximating the boundary of instability with a line), leading to

$$\frac{\mu_1 - \mu_0}{\mu_0} \simeq \frac{2(\tau_I + 1)(\tau_I + \tau_R)}{\tau_R(\tau_I + \tau_R - \tau_I^2/2)}, \tag{41}$$

where μ_0 is given by Eq. (28). In the $\tau_R \gg \tau_I$ limit,

$$\frac{\mu_1 - \mu_0}{\mu_0} \approx \frac{2(\tau_I + 1)}{\tau_R} \quad \text{as} \quad \tau_R \to \infty. \tag{42}$$

Asymptotically, we obtain the same behavior as in linear case (24). However, for small τ_R there is a significant difference between these two systems. Figure 6 shows the stability regions for the nonlinear contagion scheme for $P_k = \delta_{k,10}$ and $\tau_I = 2$. The solid line separating oscillating and fixed point solutions is obtained from the full numerical solution of Eq. (31), while the dashed curve is given by Eq. (41). We find excellent agreement. However, for $\tau_I > \tau_R$, from numerical simulations we find that Eq. (41) does not provide accurate results. Therefore, in this case we chose to determine the occurrence instability numerically. Qualitatively, the reason for this inaccuracy is that for $\tau_I > \tau_R$ we have $\mu_1 \gg \mu_0$, and

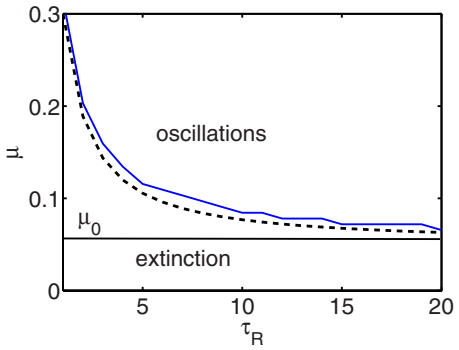

FIG. 6. (Color online) $\langle k \rangle_i^*$ as a function of the infection rate μ for $P_k = \delta_{k,10}$, $\tau_I = 2$, and $\tau_R = 2$.

first-order Taylor-expansion of a and b will no longer provide reliable results. Figure 7 shows regions of stability obtained for a power-law degree distribution with variable exponent γ, i.e., $P_k \sim k^{-\gamma}$, for $\tau_I = 4$ and $\tau_R = 2$. We applied an upper cutoff of P_k at $k = 100$. The phase portrait is shown as a function of the exponent γ and infection probability, revealing strong dependence on γ, in particular, oscillations are completely absent if γ falls below a critical value. We find that this behavior is typical of fat tailed distributions and can also be observed for $P_k \sim e^{-\alpha k}$ if $\alpha < 0.1$. We note that the numerical solution of Eq. (31) requires extra attention when $\mu \simeq 1$ because in this region the system is marginally stable, and usually a large number of time steps are necessary to determine the stability properties of the fixed point (on the order of 10^6).

V. NUMERICAL RESULTS FOR FIXED NETWORK STRUCTURE

To asses how well our annealed results apply to a fixed network structure, we implemented the SIRS model on a network consisting of 1.5×10^4 nodes for both contagion schemes. Each node on the network was initialized randomly in either a susceptible, infected, or recovered state. The time counter of the infected and recovered nodes was also set randomly between $1, \ldots, \tau_I$ and $\tau_I, \ldots, \tau_R$, respectively. After initialization, we waited 8×10^3 time steps to allow the transients related to initial conditions to relax. If we denote the time counter of a node k by $\tau_k (\tau_k \in 0, \ldots, \tau_I + \tau_R)$ and the

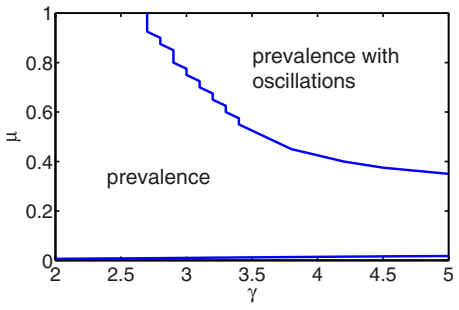

FIG. 7. (Color online) Stability regions for nonlinear contagion obtained from full numerical solution of Eq. (31), with $P_k \sim k^{-\gamma}$, $\tau_I = 4$, and $\tau_R = 2$.

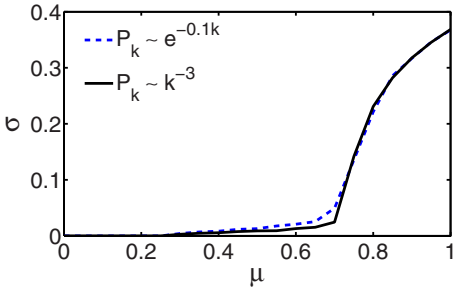

FIG. 8. (Color online) Comparison of experimental results of σ with distributions $P_k \sim e^{-0.1k}$ and $P_k \sim k^{-3}$ for $\tau_I=4$, $\tau_R=7$, and $N=1.5\times10^4$ (linear contagion).

number of nodes by N, then emergence of oscillations can be well characterized by the synchronization parameter [6–9]

$$\sigma(t) = \left| \frac{1}{N} \sum_k e^{\tau_k 2\pi i/(\tau_I+\tau_R)} \right|, \tag{43}$$

where the sum is taken over all nodes of the network except the susceptible ones ($\tau_k=0$). The appearance of persistent oscillations corresponds to synchronization of elements in the system. Their phases, τ_k, in the epidemic cycle become synchronized as the disease process proceeds. This synchronization is captured by $\sigma(t)$, which plays the role of an order parameter [6]. After transients relax, we calculate $\sigma(t)$ averaged over 200 realizations taken over a period of 2×10^3 time steps.

A. Linear contagion

For linear contagion, we demonstrate that the obtained results are independent of the degree distribution, as suggested by our annealed theory. On the other hand, we evaluate how accurately our analytical considerations predict the phase transitions between extinction and prevalence (13) and (14) and the fixed point solution and oscillatory phase (24). For a given network structure, we fix $\tau_I=4$ and we run a series of simulations for different τ_R and P_k. We find that the higher the average coordination number of the network $\langle k\rangle$, the better the agreement between our mean-field results and numerical simulations. In general, $\langle k\rangle \geq 15$ provides excellent correspondence between theory and experiment. Similarly, increasing τ_R improves the reliability of our mean-field results. We argue that the reason for this is that recovered elements in the network do not interact. The longer the recovered stage, the fewer individuals are active (susceptible or infected) at a given time instant, making the network effectively sparse. Thus, large τ_R has a tendency to diminish correlations, leading to mean-field behavior. By contrast, for $\tau_I > \tau_R$ correlations are expected to have more of an effect.

We generate uncorrelated networks for the degree distributions $P_k \sim \delta_{k,10}$, $P_k \sim \delta_{k,15}$, $P_k \sim e^{-0.1k}$, and $P_k \sim k^{-3}$. For both the exponential and the power-law cases we take $P_k=0$ for $k<10$ and $k>100$. We applied the cutoff for large connectivities to limit finite size effects. Figure 8 shows σ versus μ for two distinct distributions. The solid curve corresponds to an exponential distribution, while the dashed

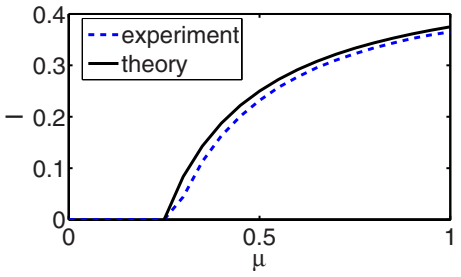

FIG. 9. (Color online) Comparison of experimental (dashed curve) and mean-field results (13) and (14) (continuous curve) for the fraction of infected individuals (I) for $\tau_I=4$, $\tau_R=4$, $P_k \sim e^{-0.1k}$, and $N=1.5\times10^4$ (linear contagion).

corresponds to a power-law distribution. Apparently, the curves are almost identical, supporting the mean-field result. Figure 9 compares the number of infected individuals as a function of infection rate for mean-field approximations (13) and (14) (solid curve) and numerical simulations (dashed curve). Again we find excellent agreement. Most importantly, the theoretical epidemic threshold, $\mu=1/\tau_I$, agrees very well with our numerical results. Figure 10 compares μ_1 (Neimark-bifurcation point) for the mean-field results with the experiments for $P_k=\delta_{k,10}$ (dotted curve) and $P_k=\delta_{k,15}$ (dashed curve) versus the time delay τ_R. Figure 10 illustrates that with increasing $\langle k\rangle$ we approach the mean-field results.

B. Nonlinear contagion

For nonlinear contagion, we first verify that the approximation given in Eq. (30) accurately gives the fraction of infected nodes. Figure 11 compares the experimental results (dashed curve) with formula (30) for $\tau_I=1$, $\tau_R=4$, and $P_k \sim k^{-4}$, indicating good agreement. Figure 12 compares the experimental results for a fixed network structure with numerical solution of annealed mean-field Eq. (31) for μ_1 (Neimark-bifurcation point). The curves are almost identical. However, if $\tau_I > \tau_R$, the mean-field approximation does not agree well with our numerical simulations. We conjecture that this can be attributed to the increased presence of correlations. While the epidemic threshold is still well characterized by Eq. (28), the Neimark-bifurcation (μ_1) displays con-

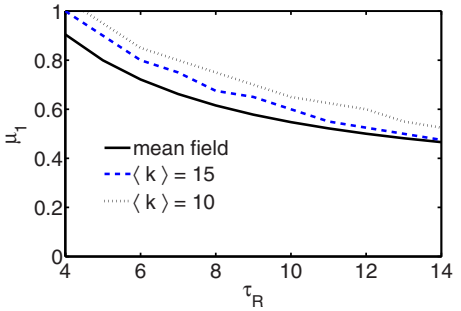

FIG. 10. (Color online) Comparison of mean-field result (24) (continuous curve) with experimental results for the Hopf-bifurcation point μ_1 as a function of τ_R for the distributions $P_k=\delta_{k,15}$ (dashed curve) and $P_k=\delta_{k,10}$ (dotted curve) for $\tau_I=4$ and $N=1.5\times10^4$ (linear contagion).

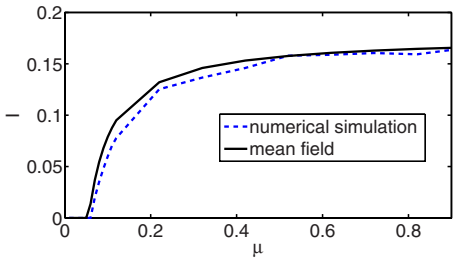

FIG. 11. (Color online) Comparison of experimental (dashed curve) and mean-field result (30) (continuous curve) for the fraction of infected individuals (I) for $\tau_I=1$, $\tau_R=4$, $P_k\sim k^{-4}$, and $N=1.5\times10^4$ (nonlinear contagion).

siderable disagreement between the annealed theory and the fixed network simulation. Figure 13 shows numerical results for μ_1 and a fixed network structure with $\tau_I=4$, $\tau_R=2$, and $P_k\sim k^{-\gamma}$ for variable exponent. Comparison of Figs. 7 and 13 reveals, unlike in mean-field theory, for a fixed network structure, small γ promotes oscillations.

VI. CONCLUSION

In this paper we have developed a mean-field theory for the discrete time-step SIRS model for the two most commonly studied contagion schemes. We found that for linear contagion the stability of prevalent, extinct, and oscillatory solutions is independent of the network structure, and the model behavior is determined exclusively by the time delays and infection probability. Numerical simulations for a fixed network structure were in excellent agreement with our theoretical predictions. By contrast, for the nonlinear contagion scheme, the epidemic threshold (μ_0) and occurrence of Neimark bifurcation (μ_1) depend strongly on the underlying network. However, the asymptotic behavior of the dimensionless quantity $(\mu_1-\mu_0)/\mu_0$ is the same for both schemes as $\tau_R\to\infty$ [Eqs. (24) and (41)]. We also found that the importance of the degree distribution is even more pronounced if the duration of infected stage exceeds τ_R, i.e., $\tau_I>\tau_R$. Referring to Fig. 7 we see that oscillations can be completely absent for power-law degree distributions with small exponents. In the case $\tau_I>\tau_R$, however, predictions of mean-field theory do not agree well with numerical simulations for a fixed network structure. We attribute this fact to correlations,

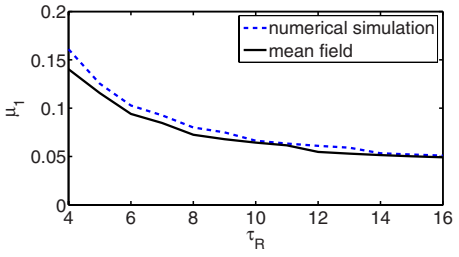

FIG. 12. (Color online) Comparison of mean-field result (24) (continuous curve) with experimental results (dashed curve) for the Hopf-bifurcation point μ_1 as a function of τ_R. $P_k\sim k^{-4}$, $\tau_I=2$, $\tau_R=4$, and $N=1.5\times10^4$ (nonlinear case).

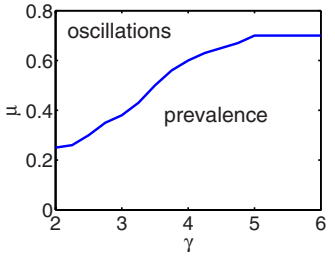

FIG. 13. (Color online) Experimental results for the Hopf-bifurcation point μ_1 for $P_k\sim k^{-\gamma}$ as a function of the exponent γ, $\tau_I=4$, $\tau_R=2$, and $N=2\times10^4$.

which are not incorporated in the mean-field approach. In summary, we have shown that the discrete time SIRS model exhibits rich dynamical behavior even within the framework of uncorrelated networks and that the contagion scheme, time delays, and infection probability play a vital role in determining model behavior.

ACKNOWLEDGMENTS

I would like thank Professor Edward Ott for his insightful comments and advice. This work was supported by the Office of Naval Research (Grant No. N00014-07-1-0734) and by the National Science Foundation (Grant No. PHY 0456249).

APPENDIX

1. Shur stability

The asymptotic stability of polynomial (21) is strongly connected to Shur's theorem. A polynomial is stable if all of its roots have absolute value smaller than 1. In general, it is possible to associate a characteristic polynomial

$$w(z)=a_0z^n+\cdots+a_{n-1}z+a_n \tag{A1}$$

with the symmetric matrix $P=S_1^TS_1-S_2^TS_2$, where

$$S_1=\begin{pmatrix} a_0 & \cdots & a_{n-2} & a_{n-1} \\ 0 & \ddots & \vdots & a_{n-2} \\ \vdots & & \ddots & \vdots \\ 0 & 0 & 0 & a_0 \end{pmatrix},\quad S_2=\begin{pmatrix} a_n & \cdots & a_{n-1} & a_1 \\ 0 & \ddots & \vdots & a_2 \\ \vdots & & \ddots & \vdots \\ 0 & 0 & 0 & a_n \end{pmatrix}.$$

The polynomial $w(z)$ is asymptotically stable if and only if the matrix P is positive definite. According to Sylvester's criterion this requirement is satisfied if all determinants associated with the upper left submatrices are positive, providing us an analytical approach to determine the stability regions of Eq. (21) as polynomials of a and b. If we denote the nth upper left subdeterminant of P with p_n, then for a given (a,b) pair $\det(p_n)>0$ for all n is a necessary and sufficient condition for stability. The curves separating the stable and unstable regions (22) and (23) correspond to $\det(p_n)=0$.

2. Linear approximation

The location where the two instability curves intersect is given by (a_0, b_0) in Fig. 2. This position can be calculated by taking the $\phi \to 0$ limit of expressions (22) and (23),

$$a_0 = \lim_{\phi \to 0} a(\phi) = \frac{\tau_I + \tau_R + 1}{\tau_I \tau_R},$$

$$b_0 = \lim_{\phi \to 0} b(\phi) = -\frac{\tau_I + 1}{\tau_R(\tau_I + \tau_R)}.$$

The derivative $db/da|_{\phi=0}$ is most easily evaluated using a symbolic mathematical software package,

$$\left.\frac{db}{da}\right|_{\phi=0} = \left.\frac{db/d\phi}{da/d\phi}\right|_{\phi=0} = \tau_I \frac{\tau_R - 1}{(\tau_I + \tau_R)(\tau_R + 1)}.$$

For the nonlinear contagion scheme Taylor expansions of $\Sigma_h h a_h$ and $\Sigma_h h a_h b_h$ with respect to the parameter μ yield

$$a = \sum_h h a_h \simeq \frac{1}{\tau_I} + \frac{\mu - \mu_0}{\mu_0} \frac{\tau_I}{(\tau_I + \tau_R)}, \tag{A2}$$

$$b = \sum_h h a_h b_h \simeq -\frac{\mu - \mu_0}{\mu_0} \frac{2\tau_I}{\tau_I + \tau_R}. \tag{A3}$$

To obtain formulas (A2) and (A3) we used the identity $\partial_\mu \langle k \rangle_i^*|_{\mu=\mu_0} = [\tau_I/(\tau_I + \tau_R)]\langle k^2 \rangle^3/(\langle k \rangle \langle k^3 \rangle)$, which is a consequence of Eq. (37).

[1] R. M. Anderson and R. M. May, *Infectious Diseases of Humans* (Oxford University Press, New York, 1991).
[2] R. Pastor-Satorras and A. Vespignani, Phys. Rev. Lett. **86**, 3200 (2001).
[3] M. E. J. Newman, Phys. Rev. E **66**, 016128 (2002).
[4] Y. Moreno, R. Pastor-Satorras, and A. Vespignani, Eur. Phys. J. B **26**, 521 (2002).
[5] M. Barthelemy, A. Barrat, R. Pastor-Satorras, and A. Vespignani, Phys. Rev. Lett. **92**, 178701 (2004).
[6] M. Kuperman and G. Abramson, Phys. Rev. Lett. **86**, 2909 (2001).
[7] D. J. Watts and S. H. Strogatz, Nature (London) **393**, 440 (1998).
[8] G. Yan, Zhong-Qian Fu, J. Ren, and Wen-Xu Wang, Phys. Rev. E **75**, 016108 (2007).
[9] Y. Kuramoto, *Chemical Oscillations, Waves, and Turbulence* (Springer, Berlin, 1984).
[10] T. Gross, Carlos J. Dommar D'Lima, and B. Blasius, Phys. Rev. Lett. **96**, 208701 (2006).
[11] L. B. Shaw and I. B. Schwartz, Phys. Rev. E **77**, 066101 (2008).
[12] M. Girvan, D. S. Callaway, M. E. J. Newman, and S. H. Strogatz, Phys. Rev. E **65**, 031915 (2002).
[13] K. L. Cooke, D. F. Calef, and E. V. Level, *Nonlinear Systems and its Applications* (Academic, New York, 1977), pp. 73–93.
[14] D. He and L. Stone, Proc. R. Soc. London, Ser. B **270**, 1519 (2003).
[15] We emphasize that the curves given by Eqs. (22) and (23) are only possible stability boundaries of Eq. (20). For example, if we cross such a curve, one of the eigenvalues typically goes from $|\lambda| < 1$ to $|\lambda| > 1$, but if one of the other eigenvalues already has $|\lambda| > 1$, then there is instability on both sides of the curve.